JOURNAL OF MATERIALS SCIENCE 26 (1991) 2229–2239

Microstructure property relationship in Pyrex glass composites reinforced with Nicalon fibres

S. M. BLEAY, V. D. SCOTT
School of Materials Science, University of Bath, Claverton Down, Bath BA2 7AY, UK

Detailed microstructural studies have been carried out on a series of composites consisting of Pyrex glass reinforced with Nicalon fibres. A variety of techniques has been employed, including X-ray and electron diffraction, electron-probe microanalysis and thin foil analytical electron microscopy. In parallel, mechanical tests have been performed on the composites and measurements have been made of the fibre–matrix bond.

Substantial amounts of cristobalite have been identified in the matrix, up to ~48% by volume in some cases. At such levels, microcracking is a common occurrence due to the high differential contraction between the matrix constituents upon cooling, which leads to matrix disintegration upon mechanical testing. A second microstructural feature which affects the mechanical behaviour of the composite concerns the fibre–matrix interface and, in particular, the chemistry of the outermost (~200 nm) surface regions of the fibre. The amount of graphite here is shown to affect directly the strength of the fibre–matrix bond and, in turn, the degree of fibre pull out and the mechanical properties of the composite.

1. Introduction

Many potential applications of glassy materials are limited by their inherently brittle nature and their tendency towards catastrophic failure. Such characteristics, which result in far lower (< 100 MPa) strengths than would be expected from theoretical predictions (several 1000 MPa), can be attributed to the presence of small defects such as cracks which act as stress concentrators. One approach to improve the mechanical properties of glass is to alter the failure mode from catastrophic to controlled fracture by, for example, reinforcing the glass with high modulus fibres. With such a composite structure promising results have been achieved, including improved fracture toughness and strengths in excess of the parent glass matrix. Hence, when coupled with their potentially high specific stiffness and strength and their retention of properties up to temperatures higher than is feasible with metals, they become attractive candidates for aerospace applications.

Early studies by Sambell, Bowen and Phillips [1–3] on glass and glass–ceramics reinforced with carbon fibres showed that Pyrex gave the more satisfactory results, although the potential of the system was limited by the response of the carbon fibre reinforcement to oxidation. Later, a silicon carbide type of fibre, developed by Yajima *et al.* [4, 5] and manufactured commercially under the name of Nicalon*, was investigated by Prewo and Brennan [6, 7] for reinforcing Pyrex. Promising results were obtained and since then various aspects of this system have been studied by a number of workers [8–10].

This paper is concerned with an investigation of Pyrex glass reinforced with Nicalon fibres. It involves a detailed microstructural study using a variety of techniques, including optical and analytical electron microscopy, and parallel mechanical tests which include the measurement of the fibre–matrix interfacial bond strength. The respective roles of the matrix, fibre and fibre–matrix interface are then discussed.

2. Experimental procedure

2.1. Materials

Several batches of Pyrex glass reinforced with Nicalon fibres have been investigated. They were supplied as plates and manufactured by hot pressing at 950 °C [8]. The origin of the composite materials and their batch designations are given in Table I; batches A1, A2 and A3 were supplied by AEA, Harwell, and B1 by Rolls Royce plc.

Nicalon fibre coated with glass particles in a slurry bath to form a "prepreg" sample was also studied, as well as raw materials in the form of Pyrex tubing, ball-milled Pyrex powder, and sized Nicalon fibre tow, all of which were supplied by AEA, Harwell.

2.2. Mechanical tests

Tensile tests of the composites were conducted on an Instron model 1195 using a crosshead speed of 0.5 mm min^{-1}. All test specimens were rectangular in shape, see Table 1. Batches A1 and A3 were 100 mm long by 10 mm wide by 2 mm thick, and had

* Nippon Carbon Co.

0022–2461/91 $03.00 + .12

TABLE I Origin and dimensions of test specimens

Plate designation	Layup	Origin	Tensile test dimensions[a] (mm^3)	Three-point bend l/t ratio
A1	ud	AEA Harwell	50 × 10 × 2	25:1
A2	ud	AEA Harwell	40 × 5 × 1	20:1
A3	$[0°, 90°]_{3s}$	AEA Harwell	50 × 10 × 2	25:1
B1	ud	Rolls Royce	80 × 20 × 2	—

[a] Average values.

aluminium end tabs glued with epoxy resin to leave an effective gauge length of 50 mm. Specimens in batch A2 were smaller, 100 mm long by 5 mm wide by 1 mm thick, and had glass fibre–epoxy end tabs to give an effective gauge length of 40 mm. Batch B1 specimens were 100 mm long by 20 mm wide by 2 mm thick, and had aluminium end tabs with a gauge length of 80 mm.

Three-point bend tests were carried out, at the same crosshead speed, using specimens of the same width and thickness as those used for tensile testing; length to thickness ratios are included in Table I.

All test specimens were cut from composite plate using a resin-bonded diamond wheel and their edges ground on silicon carbide paper to give a smooth finish.

2.3. Interface friction measurements

Measurements of the interfacial friction stress between fibre and matrix of the composites were made using the technique developed by Marshall [11]. A polished transverse section through a unidirectional composite was first prepared (see Section 2.4). A microhardness indenter was then applied to the centre of the fibre to produce depression of the fibre below the level of the surface. For a particular fibre diameter, the load applied was chosen so that the hardness indentation extended from the fibre into the surrounding glass matrix. The friction stress was then calculated from the equation

$$\tau = F^2/4\pi^2 u R^3 E_f$$

where R is the fibre radius, E_f the fibre modulus (E_f = 200 GPa) and F the force applied to the fibre. The term, u, is the fibre depression at maximum load and it is measured from the geometry of the indentation mark in the glass matrix.

Loads varying from 0.25 to 2.0 N were applied to fibres of diameters ranging from 10 to 35 μm, using a LECO M-400 hardness tester.

2.4. Microstructural examination

Polished sections of composite were prepared by first cutting a sample from a plate using a resin-bonded diamond wheel at low speed and then mounting it in "Epofix" cold curing resin. Sections were ground flat using a diamond grinding wheel lubricated with water and a force of 22 N per sample. Polishing was achieved in three further stages. Firstly,10 min on a Buehler Metlap 4 wheel with 6 μm diamond slurry, with the wheel contra-rotating at 25 r.p.m.; secondly, 10 min on a Buehler Metlap 2 wheel with 6 μm diamond slurry, the wheel contra-rotating at 120 r.p.m.; finally, 10 min on a Buehler Metlap 1 wheel with 1 μm diamond slurry and "Silco" colloidal silica, followed by a further minute with a water wash. This polishing routine was found to give little matrix damage and no visible fibre pullout.

Optical microscopy was carried out on a Zeiss ICM 405 using Nomarski interference. Examination in the scanning electron microscope (SEM) required first coating the samples with a conducting layer of gold or carbon; a JEOL T330, or a JEOL 35C microscope fitted with backscattered electron imaging (BEI) was used. Compositional analysis of microstructural features was achieved with a LINK AN10000 energy-dispersive X-ray spectrometer (EDS) attached to the JEOL 35C or with a JEOL JXA-8600 fitted with four wavelength-dispersive X-ray spectrometers (WDS). SEM was used also to study individually mounted Nicalon fibres after first burning off the size, composite sections after etching in 5% HF for 2.5 h, and tensile fracture surfaces of composite plates. A thin coating of gold was always needed.

Thin foil specimens for transmission electron microscopy (TEM) were fabricated from bulk material in the following way. A 3 mm diameter disc was cut using a diamond tipped coring drill and ground to ~ 300 μm thickness on 400 grit SiC paper. The disc was then placed on a VCR Model D500 and "dimpled" on both sides to produce a central specimen thickness of ~ 20 μm. Final thinning was achieved by argon-ion bombardment in a Gatan Duomill firstly at 5 kV with an incidence angle of 15° until perforation of the sample occurred, and then using an angle of 7° to extend the area of thinned material. TEM examination was carried out using a JEOL 2000FX instrument fitted with a LINK AN 10000 EDS system with high-angle thin-window X-ray detector. As well as using the bright field mode, selected area diffraction (SAD) and EDS analysis was carried out.

Samples of each composite plate were ground into powder and examined by X-ray diffraction (XRD) in a Philips PW 1820/00 diffractometer. Similar powder diffraction studies were carried out on Pyrex glass, Nicalon fibre and prepreg material. A quantitative measure of the degree of crystallinity present in the glass matrix was obtained by reference to a calibration curve constructed using standards of known composition. The standards were produced by mixing ball-milled Pyrex powder and α-cristobalite powder (obtained from Hepworth Minerals and Ceramics

Ltd) in the following volume percentages: 0:100, 12.5:87.5, 25:75, 37.5:62.5, 50:50, 62.5:37.5, 75:25, 87.5:12.5, 100:0. To these were added 40% of ground Nicalon to take account of the fibre content of composite plates and 50 wt % of α-Al_2O_3 as an internal reference (12). The diffraction peak at $2\theta = 22.05°$ (101 reflection from α-cristobalite) and $2\theta = 66.8°$ (124 reflection from α-alumina) were selected for analysis, where θ is the Bragg angle. The ratio of these diffraction peaks for the standards was then plotted against known volume % cristobalite to produce the calibration curve.

Cristobalite contents of the composite plates were deduced by mixing ground samples with 50 wt % α-Al_2O_3, and measuring diffraction peak ratios as above and then reading off the content from the calibration curve.

Results

3.1. Starting materials

SEM micrographs of a sample of Pyrex glass tubing were featureless, whether taken in the secondary electron mode (SEI) or BEI, indicating that the as-received glass was homogeneous. EDS gave the composition as 35 ± 2 wt % silicon, 55 ± 2 wt % oxygen, 3.5 ± 0.5 wt % sodium and 1.5 ± 0.5 wt % aluminium; the balance of ~ 5 wt % boron; the constituents were uniformly distributed. TEM of a thin foil of Pyrex glass together with SAD showed that the matrix was amorphous as well as homogeneous.

Ball-milled Pyrex powder had an angular morphology, with particle sizes ranging from 2 to 30 μm and an average size of 10 μm. XRD of the ball-milled powder, Fig. 1, shows a very broad diffraction peak typical of an amorphous material, whilst EDS in the SEM substantiated that it was composed of oxygen, sodium, aluminium and silicon, as recorded on an as-received Pyrex glass.

Nicalon fibre was seen to have a smooth surface after removal of the size, Fig. 2, and EDS showed it to consist of silicon, carbon and oxygen. EPMA of a polished section through A1 Nicalon fibre using the JEOL JXA-8600 gave a bulk analysis of ~ 33 wt % carbon, ~ 58 wt % silicon, ~ 9 wt % oxygen and 0.3 wt % sodium, equivalent to ~ 50 at % carbon, ~ 40 at % silicon, ~ 10 at % oxygen and 0.5 at % sodium. The XRD pattern of powdered Nicalon fibre, Fig. 1, shows two weak broad peaks which are characteristic of amorphous rather than crystalline material, the degree of microcrystallinity which characterizes Nicalon (see later) being undetectable by this technique.

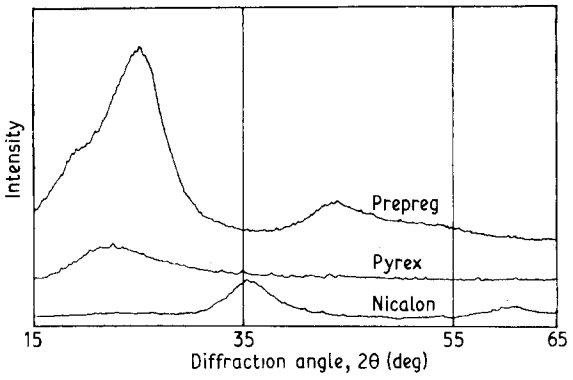

Figure 1 X-ray diffraction from starting materials.

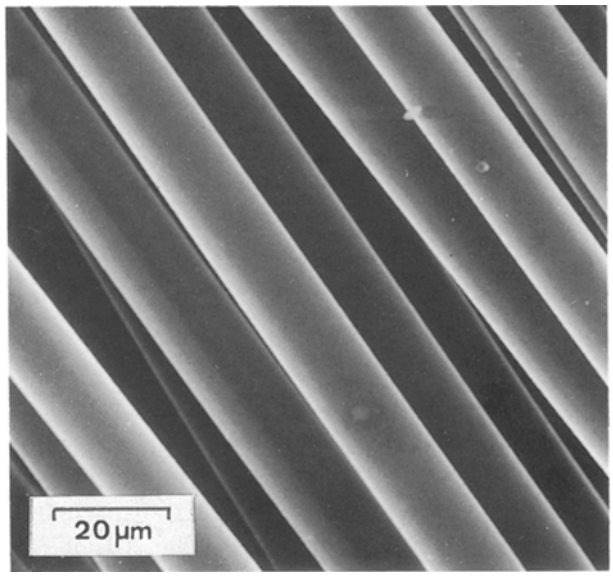

Figure 2 Nicalon fibres after removal of size, SEM.

An SEM picture of prepreg material, Fig. 3, shows the polymeric binder picked up by the fibre upon winding through the slurry bath as a "streaking" effect on the fibre surface. EDS of the surface identified the major element present as carbon from the polymeric binder, with some traces of oxygen, aluminium and silicon. XRD of a powdered prepreg sample showed it to be essentially amorphous. The broad Pyrex peak at $2\theta \approx 25°$ is just visible and there are, in addition, diffuse peaks at $2\theta \approx 25°$ and 44° attributable to the polymeric binder.

3.2. Mechanical tests

Mechanical test results, Table II, show that batch A1 of undirectional composite is inferior to batch A2. The

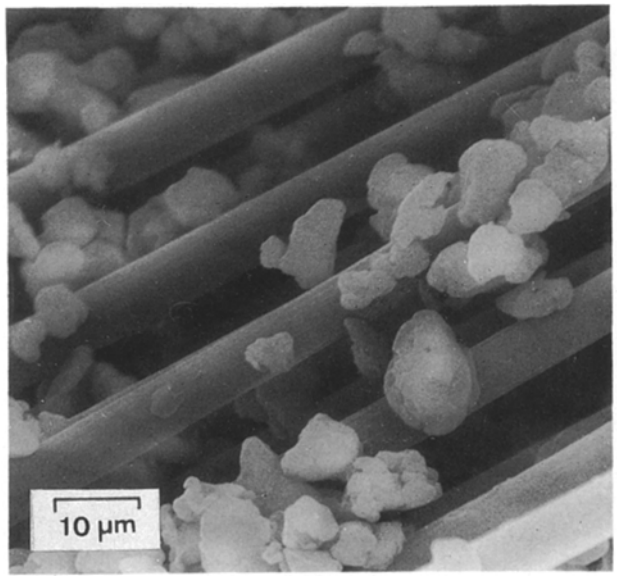

Figure 3 Prepreg material, SEM.

TABLE II Properties of composites

Material	Fibre (vol %)	Tensile strength (MPa)	Flexural strength (MPa)	Interface bond strength (MPa)	Cristobalite (vol %)
A1	47 ± 5	330 ± 10 (5)	530 ± 40 (5)	8.2 ± 3.7 (25)	48 ± 3
A2	27 ± 5	390 ± 35[a] (7)	880 ± 100 (11)	4.1 ± 1.0 (40)	11 ± 3
A3	46 ± 5	170 ± 60 (5)	300 ± 40 (5)	–	34 ± 3
B1	42 ± 5	725 ± 65[b] (4)	–	2.0 ± 0.5 (20)	45 ± 3

[a] Ford *et al.* [9].
[b] Habib *et al.* [13].
Figures in parentheses refer to number of tests.

tensile strength of A1 is 330 ± 10 MPa, compared with 390 ± 35 MPa for A2, but the difference is more evident in the measured flexural strengths of 530 ± 40 MPa for A1 and 880 ± 100 MPa for A2. The crossply plate A3, fabricated in the same batch as A1, had tensile and flexural strengths of 170 ± 60 and 300 ± 40 MPa, respectively, appropriately half the A1 values as might be expected from its crossply structure. The tensile strength of composite B1 was significantly higher than that of the other batches, at 725 ± 65 MPa [13].

3.3. Interface friction measurements

Fig. 4a shows an indented fibre in specimen A1, where the force required to start the fibre sliding has caused damage to the surrounding matrix. With A2, Fig. 4b, less force was required to depress the fibre and little matrix damage is seen. Results of micro-indentation experiments are collated in Table II. The interfacial friction stress of A1 was estimated as 8.2 ± 3.7 MPa, whilst that for A2 was 4.1 ± 1.0 MPa. The interfacial friction stress of 2.0 ± 0.5 MPa for batch B1 was the lowest of the three samples tested in this way.

3.4. Microstructure of composites

3.4.1. Optical microscopy

Optical microscopy showed clear microstructural differences between each batch of material.

Composite plate A1, Fig. 5a, had a non-uniform distribution of fibres which still retained their arrangement in tows; in some cases the fibres were so closely packed as to be in contact. The volume fraction of fibres was estimated from a series of representative micrographs as 0.47 ± 0.05. The glass matrix showed a fine structure, the Nomarski interference contrast mode giving the fibres a raised and rounded appearance. Composite A3 had a more uniform distribution of fibres, Fig. 5b, but a similar fibre volume fraction of 0.46 ± 0.05. A fine structure was again visible in the glass matrix. The structure of A2 differed in several respects from the two above. Firstly, there was a large variation in fibre diameter ranging up to 45 μm, compared with an average value of ~ 12 μm. Secondly, the fibre volume fraction was only 0.27 ± 0.05 although the distribution was more homogeneous. Thirdly, although fine microstructural features were again visible in the matrix, they were less numerous. In plate B1, the fibres were fairly uniform in size, had a homogeneous distribution and a volume fraction of 0.42 ± 0.05. Many fine features were observed in the matrix.

3.4.2. Scanning electron microscopy

The microstructure of the glass matrix is seen more clearly in Fig. 6a, taken from A1 using the backscattered electron imaging (BEI) mode of the SEM.

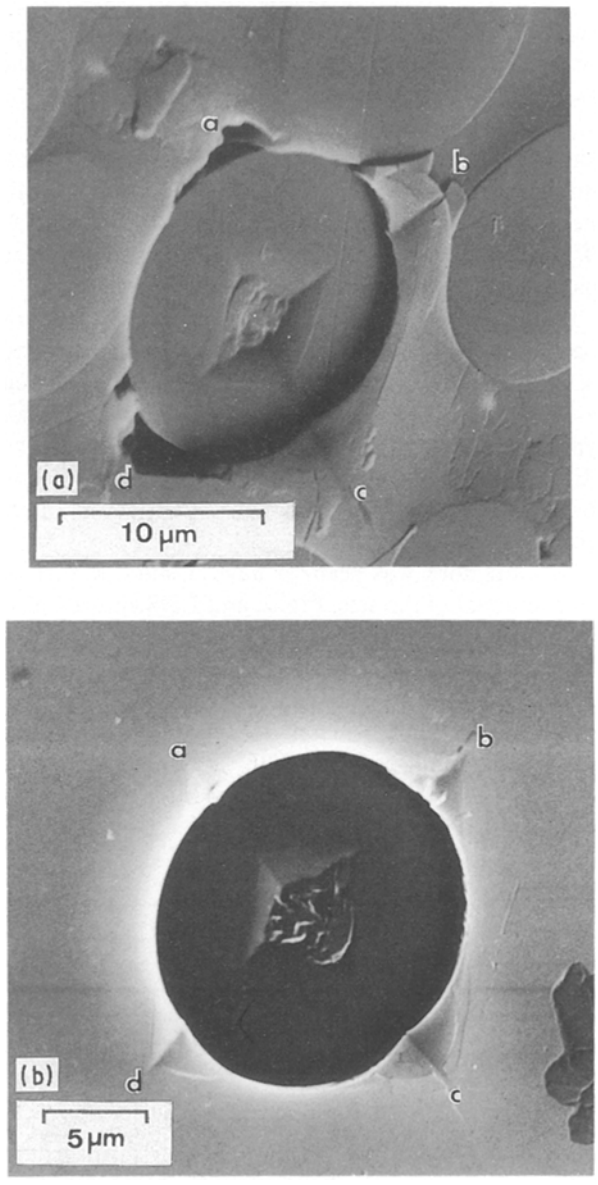

Figure 4 Microhardness indentations on fibres, SEM; the indentor depresses the fibre and makes contact with the matrix to give the indentation marked (a), (b), (c) and (d). (a) Composite A1, (b) Composite A2.

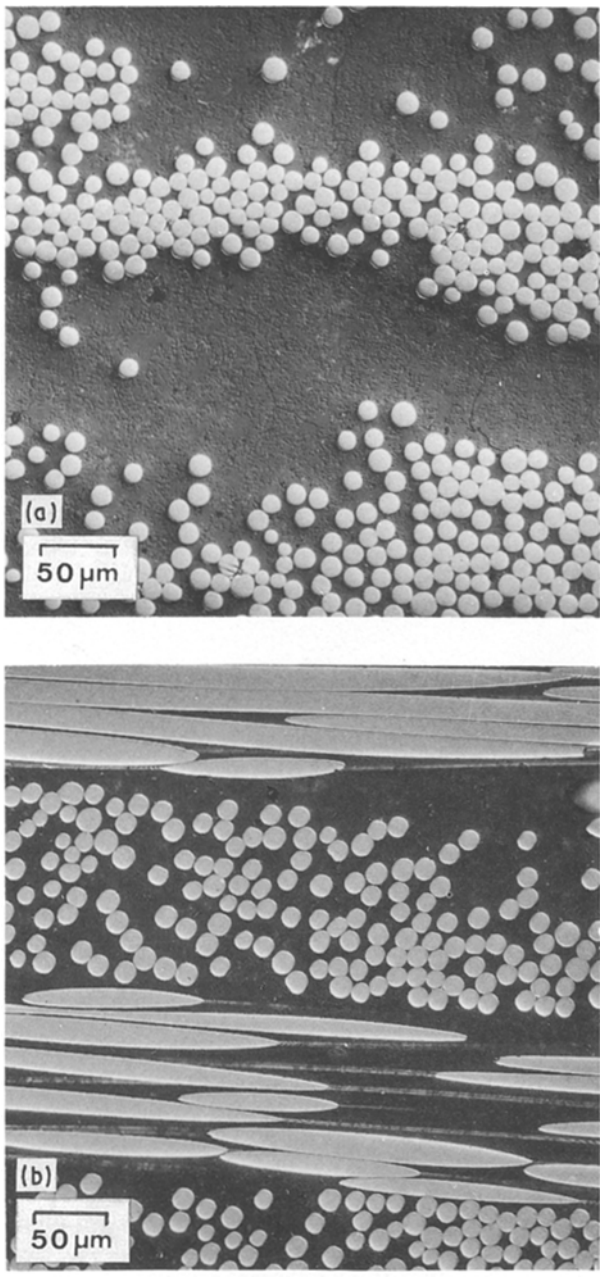

Figure 5 Polished sections, OM (a) Composite A1, (b) Composite A3.

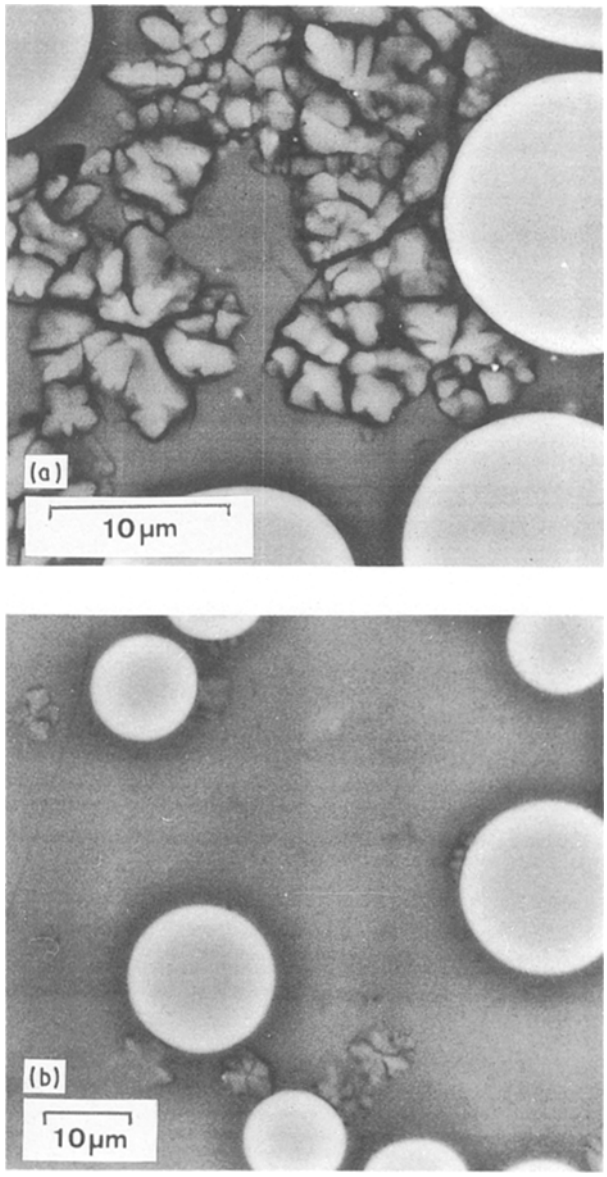

Figure 6 Polished sections, SEM backscattered images. (a) Composite A1, note the large amount of second phase in the matrix. (b) Composite A2, containing small amount of second phase.

Rosette-like structures are resolved, the degree of backscattered image contrast indicating that their mean atomic number is higher than that of the surrounding matrix. The BEI mode also reveals the presence of microcracking in the second phase regions. In contrast, sample A2 contained much less matrix second phase and microcracks could not be found, Fig. 5b.

EDS, obtained using the attachment to the SEM, showed that the matrix of both A1 and A2 contained 35 ± 3 wt % silicon, 50 ± 3 wt % oxygen, 3 ± 0.5 wt% sodium and 2 ± 0.5 wt% aluminium, in accordance with the Pyrex specification. Little difference in chemical composition was apparent between a second-phase particle and the surrounding matrix but this was later found to be due to the difficulty of confining such analyses to a single particle of this shape complexity. After removal of much of the surrounding matrix by etching the specimen in 5% HF solution for

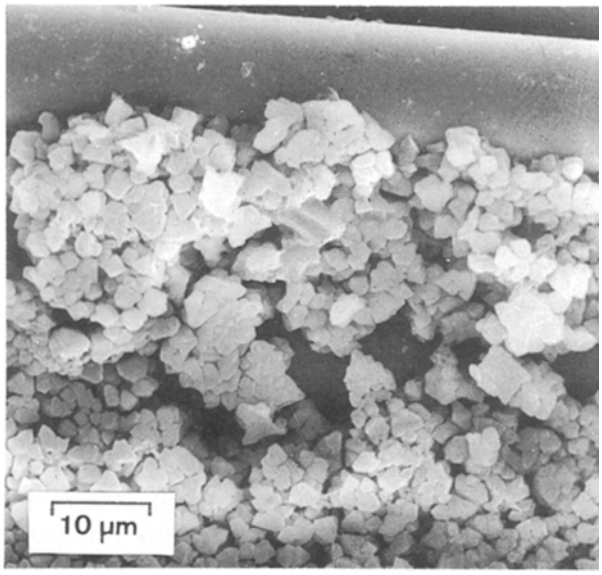

Figure 7 Composite B1, etched in HF solution to show second phase, SEM.

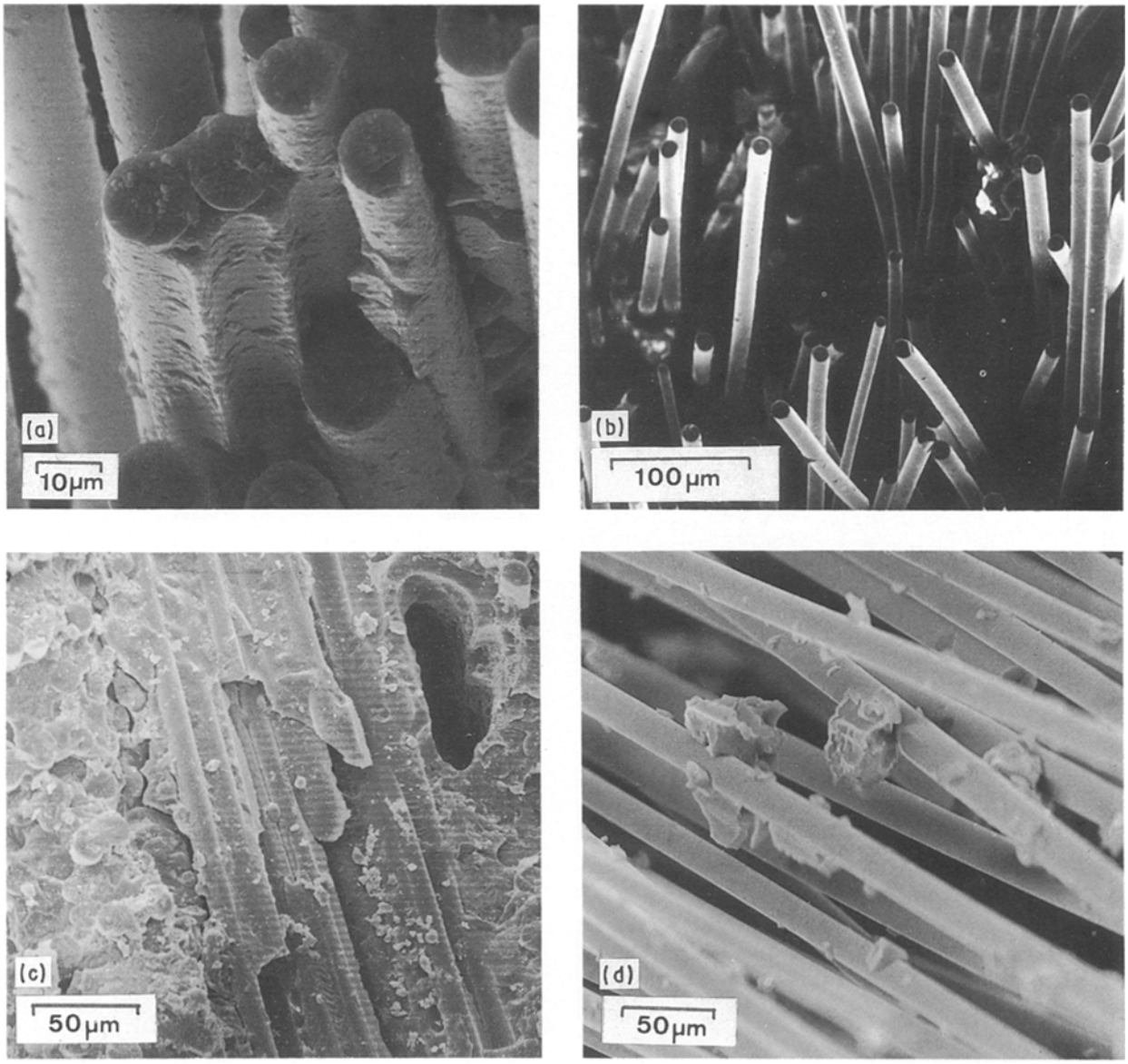

Figure 8 Fracture surfaces, SEM (a) Composite A1, (b) Composite A2, (c) Composite A3, (d) Composite B1.

2.5 h, Fig. 7, the EDS analysis was repeated, whereupon it was revealed that the second-phase particles contained mostly silicon and oxygen, with a trace (~ 0.5 wt %) of aluminium and no detectable sodium (< 0.2 wt %). Note that in etched specimen B1, the second-phase particles, whilst discrete, seem to form an almost continuous network throughout the matrix.

3.4.3. Fractography

Examination of fracture surfaces in the SEM indicated that each batch of composite failed in a different way.

The tensile fracture surface of A1, Fig. 8a, is characteristic of a predominantly brittle condition. Where fibre pullout did occur the pullout length was no more than 200 μm and the fibres themselves had many adherent particles. Similarly brittle behaviour was exhibited by crossply plate A3, Fig. 8b. Fibre pullout here is limited to ~ 50 μm and porosity can be observed in the matrix-rich regions between perpendicularly aligned fibres. The fracture surface of A2, Fig. 8c, shows more extensive fibre pullout, approaching lengths of several 100 μm but the surface of exposed fibres is smooth with no adherent particles. In the case of B1, the matrix exhibited severe and progressive disintegration well below the peak loading of 725 $\pm$ 65 MPa. Long lengths of fibre were exposed, Fig. 8d, the surfaces of such fibres being generally free of adherent particles, apart from an occasional "collar" of glass matrix.

3.4.4. Thin foil studies

The transmission electron micrograph of a thin foil of B1 illustrated in Fig. 9a was obtained from the matrix. The SAD pattern from region I in the micrograph (Fig. 9b) indicates it to be amorphous whilst the corresponding EDS data, Fig. 9c, showed that its chemical composition accords with that of Pyrex. Region II gives a single-crystal diffraction pattern, Fig. 9d, which can be indexed on the basis of α-cristobalite, a tetragonal structure with $a = 0.4971$ nm and $c = 0.6918$ nm. The crystalline phase is a polymorph of silica, Fig. 9e, and is identifiable with the rosette-like constituent referred to earlier. Microcracks can be seen to originate at the interface between

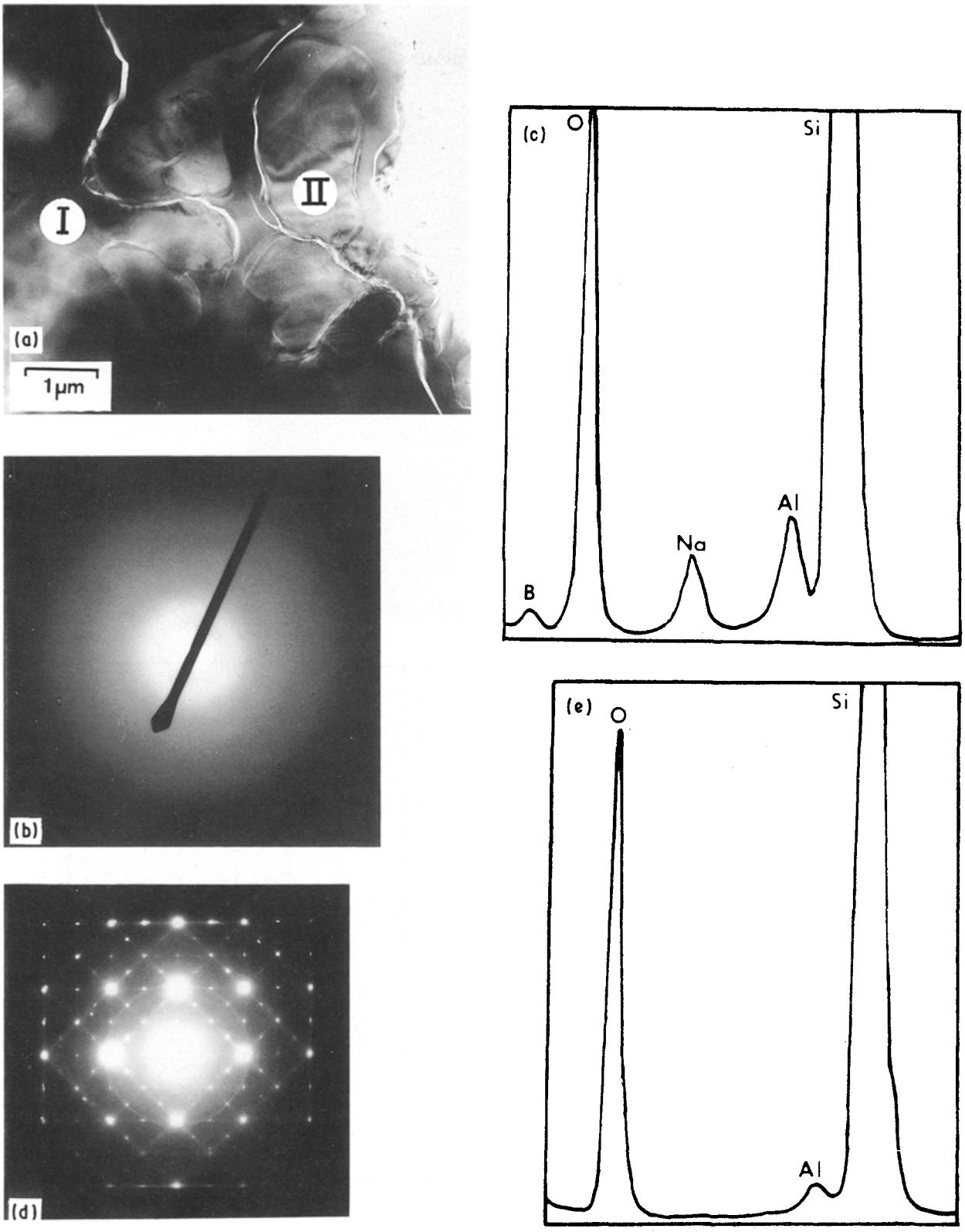

Figure 9 Matrix of composite B1. (a) TEM showing second phase and cracks, (b) SAD from region I, (c) EDS from region I, (d) SAD from region II, (e) EDS from region II.

the regions of α-cristobalite and the glassy phase and to extend into the matrix. Traces of β-cristobalite were sometimes found mixed with the α phase.

Fig. 10a was taken from a section of specimen A1 which included the fibre–matrix interface. The surface zone (~ 250 nm thick) of the fibre appears more electron transparent than the rest. A selected area diffraction pattern, Fig. 10b, from the fibre interior (region I) consists of fairly diffuse rings indicative of microcrystalline β-SiC. The corresponding EDS data, Fig. 10d, show that in addition to silicon and carbon, appreciable oxygen (~ 10 wt %) is present and a small amount of sodium (< 1.0 wt %). The surface zone (Region II) has an amorphous structure, Fig. 10c, and a chemical composition, Fig. 10e, which is significantly different from the rest of the fibre; the levels of

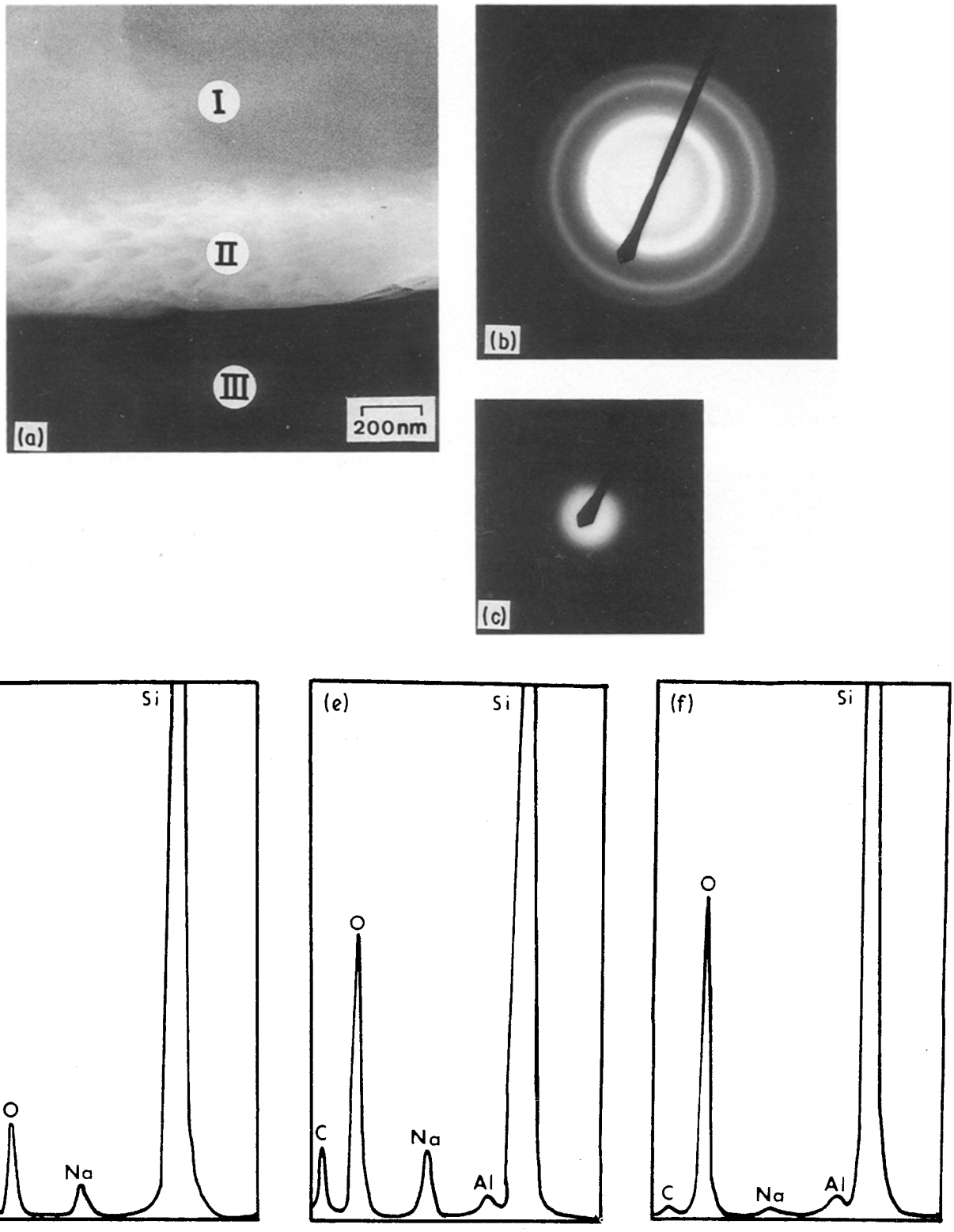

Figure 10 Fibre–matrix interface of composite A1. (a) TEM, showing fibre (I) surface zone (II) and matrix (III) (b) SAD from region I, (c) SAD from region II, (d) EDS from region I, (e) EDS from region II, (f) EDS from region III.

oxygen (~ 30 wt %) and sodium (~ 5 wt %) are higher and the carbon content correspondingly lower (~ 8 wt %).

The region of the adjacent matrix (III) also had an amorphous structure (cf. Fig. 9b). Its chemical composition showed a small depletion of sodium, Fig. 10f, otherwise it was the same as the Pyrex. The very small carbon peak visible in the matrix spectrum may be due to some surface contamination of the thin section, either during preparation or while it was being examined in the TEM, or may be caused by diffusion of carbon out of the fibre during manufacture.

The structure of the fibre–matrix interface B1, Fig. 11a, is different in appearance from that of A1. A region of lighter contrast, ~ 100 nm thick, is again visible at the fibre surface, but the texture is not the same. EDS of regions of fibre (I) and matrix (III) gave similar data to those in Figs 10d and 10f, but the interfacial region (II), Fig. 11b, has several distinguishing features. Sodium enrichment of the interface is

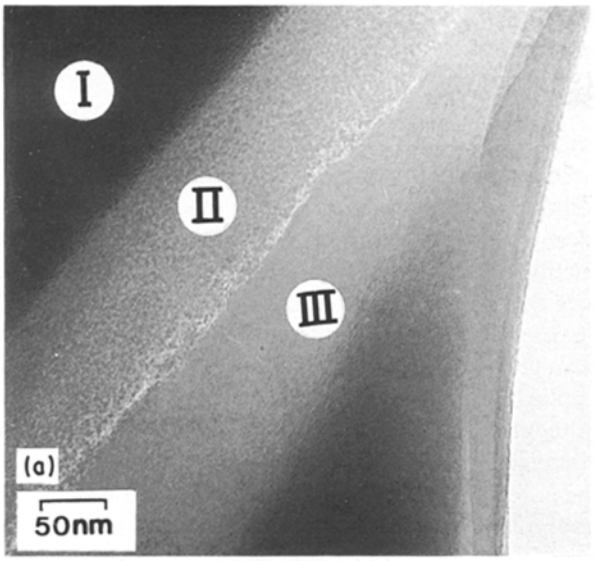

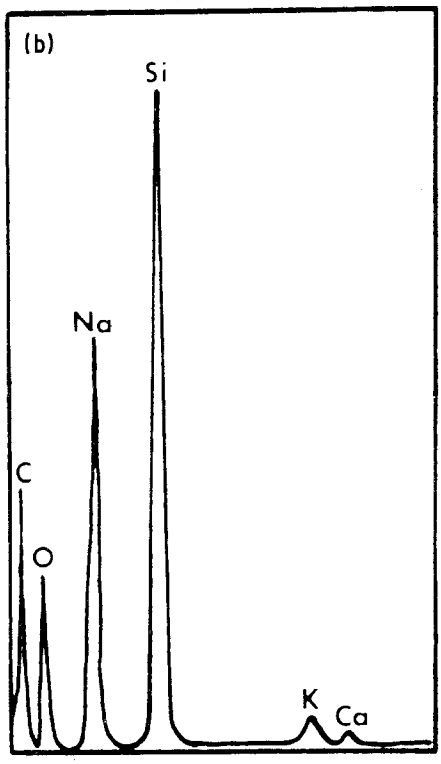

Figure 11 Fibre–matrix interface of composite B1. (a) TEM, showing fibre (I) surface zone (II) and matrix (III), (b) EDS from surface zone.

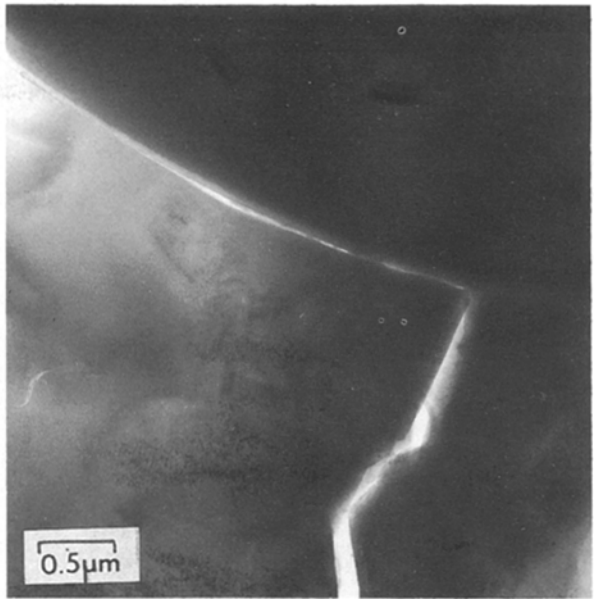

Figure 12 Fibre–matrix interface of composite A2, showing crack deflection around fibre, TEM.

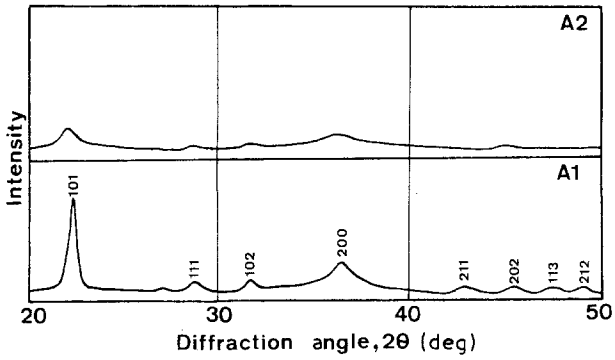

Figure 13 X-ray diffraction peaks from composites A1 and A2, showing different α-cristobalite contents.

greater (~ 10 wt %) than in A1 and traces of potassium and calcium are seen. Carbon segregation was a feature of this interface, and this element is believed to be concentrated in the outer 10 nm of the fibre surface, giving the lighter contrast.

Fig. 12 illustrates an interface of A2 showing initiation of a crack in a cristobalite region in the matrix, its propagation towards an interface, and its deflection around the fibre. The chemical composition of the interface was found to be similar to that of A1.

3.4.5. X-ray diffraction studies

XRD traces, Fig. 13, show peaks indexed as α-cristobalite in A1 and A2. Quantitative estimates of cristobalite content in the four batches were: A1 48 ± 3 vol %, A2 11 ± 3 vol %, A3 34 ± 3 vol %, and B1 45 ± 3 vol %, see Table II.

4. Discussion

4.1. The composite components

The structure and composition of the as-received Pyrex glass was typical of this class of material with ~ 50 wt % silicon, 1.5 wt % aluminium, 2.5 wt % sodium, 40 wt % oxygen, and the balance boron. It was amorphous and remained so prior to the hot pressing operation. Nicalon fibres were smooth with an average diameter of 12 μm but ranging up to 45 μm. EPMA showed they consisted of ~ 33 wt % carbon, ~ 58 wt % silicon, ~ 9 wt % oxygen and ~ 0.3 wt % sodium, which equates with ~ 50 at % carbon, ~ 40 at % silicon, ~ 10 at % oxygen and ~ 0.5 at % sodium. SAD in the TEM identified microcrystalline β-SiC as a constituent. Hence, if it is assumed that the oxygen which was present was combined with silicon, as SiO_2 and/or non-stoichiometric silicon oxycarbide (SiO_xC_y) as suggested by other workers [14, 15], then some of the carbon present

must exist as free carbon. The traces of sodium impurity which were detected probably originated from the fibre manufacturing process.

4.2. The glass matrix

After hot pressing into composite plates, crystallization of the glass matrix was detected. The crystalline phase was identified as α-cristobalite, a silica polymorph. In some instances, traces of β-cristobalite, the high temperature form, were found. The cristobalite was present as discrete, irregularly shaped particles which were distributed throughout the glassy matrix; at high concentrations they formed a virtually continuous network. There was no evidence to suggest that Nicalon fibres had played a crucial role in the formation of the cristobalite phase, as had been proposed by Murty and Lewis [16]. Some cristobalite was indeed located at the fibre interface, but this would have been expected with such a high volume of more-or-less randomly distributed particles.

The formation of cristobalite in the composite plate would be favoured by one or more of three processing factors. Firstly, the composite pressing temperature of $\approx 950\,^{\circ}C$, lies in the optimum recrystallisation temperature range for Pyrex. Secondly, the application of pressure would promote the formation of cristobalite, a more dense constituent than either Pyrex or the alternative silica polymorph, tridymite. Thirdly, calcium-containing impurities were found in the ball-milled powder which would provide suitable nucleation sites for cristobalite, as previously found for sintered Vycor glass [17].

The microcracking which is associated with the cristobalite regions results from the different thermal expansion coefficients of Pyrex glass and cristobalite as follows. Cristobalite would form at the hot pressing temperature of 950 °C and, during cooling the material to $\sim 600\,^{\circ}C$, the thermal contraction stresses would be relieved by viscous flow of the glass. When the glass solidification temperature was reached, the stress, which will be tensile in the Pyrex, would increase until relieved by crack formation at or close to the Pyrex–cristobalite interface. A further volume contraction with a corresponding increase in the stresses generated upon cooling would arise when at $\sim 277\,^{\circ}C$ the β-cristobalite transformed to the α phase.

The amount of cristobalite in the different composite plates was found to vary from 48 ± 3 vol. % for A1 to 11 ± 3 vol % in the case of A2. Their corresponding tensile strengths were 330 ± 10 MPa and 390 ± 35 MPa, and flexural strengths were 530 ± 40 MPa and 880 ± 100 MPa. Hence, it may be concluded that large amounts of cristobalite were detrimental to composite properties since the microcracks, which almost inevitably form, link together to form a network of cracks which cause disintegration of the matrix.

4.3. The fibre–matrix interface

The cristobalite content is, however, not the only factor to be considered with regard to the mechanical strength of a composite since, although A1 and B1 had similar cristobalite concentrations (48 ± 3 vol % and 45 ± 3 vol %), their tensile strengths were markedly different (330 ± 10 MPa and 725 ± 65 MPa). Fractography results help explain these effects.

In the case of specimen A1, there was limited fibre pullout and particles of matrix material were commonly found adhering to the fibre. Furthermore, the friction stress measured at the fibre–matrix interface was the highest of the three specimens tested, at 8.2 ± 3.7 MPa. These results are all consistent with a strong fibre–matrix bond. Thus when a stress was applied to the composite, the pre-existing microcracks in the matrix propagated across the specimen, as in a completely brittle material, with little recognition of the fibre–matrix interface. This implies that fibres were fractured before they reached their tensile strength. The fibre–fibre contact due to close packing in the tows may also contribute to the brittle failure mode.

With composite B1, the bond was weak (interface friction stress of 2.0 ± 0.5 MPa) and long and generally clean lengths of fibre were exposed in the mechanical test. Evidence was also available showing that the pre-existing matrix microcracks were deflected at the weak fibre–matrix interface to give a three-dimensional network of cracking which then led to the observed matrix fragmentation. The fibres remained more or less intact, however, and could support some load, the measured strength being 725 ± 65 MPa. If the rule of mixtures is applied, and taking tensile strengths of 2 GPa for the fibre and 100 MPa for the glass matrix, this value would imply that either only ~ 45% of the fibres were load bearing or fibre strength has been degraded during composite manufacture.

The importance of an optimum fibre–matrix bond strength such that crack deflection at the interface is encouraged is also evidenced in composite A2. The interface friction stress was 4.1 ± 1.0 MPa, not as low as that measured for composite B1 but sufficient to allow some degree of fibre pull out. This composite had, however, the lowest concentration of cristobalite and the combination of these two microstructural characteristics produced a material with good mechanical properties. For example, its flexural strength of 880 ± 100 MPa was well in excess of that of either A1 or A3, whilst its recorded tensile strength of 390 ± 35 MPa was also superior especially when allowing for a much smaller volume fraction of fibre (~ 0.27 ± 0.05 compared with almost 0.5 for the other three composite plates). This correlation between interface friction stress and observed micromechanics of the fracture process has also been noted by Tredway *et al.* [18] in their work on Pyrex glass reinforced with carbon fibres. They further found that different additions to the glass matrix caused changes in interface bond strength and the mode of fracture of the composite.

In the present work, some differences in the microstructural characteristics of the fibre–matrix interface were found which may be related to the measured interfacial bond strengths. Let us then consider the structures of composites A1 and B1, since these had

the highest (8.2 ± 3.7 MPa and the lowest (2.0 ± 0.5 MPa) respective interface bond strengths. Both fibres, it was observed, had a thin (< 200 nm thick) surface layer with a crystal structure and chemical composition which was different from the remainder of the fibre. These layers were amorphous and rich in oxygen (~ 30 wt %) and are considered to have been present before the fibres were incorporated into a composite. Thus, the sodium they contain, between 5 and 10 wt %, and much more than the trace left behind (~ 0.5 wt %) after fibre manufacture, results from diffusion from the surrounding glass matrix, to leave the regions found denuded in sodium. Hence the sodium ions, which are not strongly bound in the glass network, diffuse readily into the zone of amorphous silica but not, to any degree, into the microcrystalline regions of the Nicalon fibre. The identification of an amorphous silica layer would accord with the findings of Clark *et al.* [19] using the ESCA technique.

With regard to the composition of the fibre surface layers, the first feature of note concerns the level of sodium absorbed in these regions. This was significantly higher in B1 where the interfacial bond was weaker. Another important difference concerned the carbon present at the fibre–matrix interface which was very much greater at the weaker interface, ~ 15 wt % in B1 compared with 8 wt % in A1. Finally, some traces of potassium and calcium were found at the weak interface. Since the chemistry of the surface layer would undoubtedly play an important role in connection with fibre–matrix bond strength, it may be argued that such chemical differences may well account for the difference in interfacial friction stresses of composites A1 and B1. It is proposed that the higher interface friction stress measured in A1 is associated with the stronger fibre–matrix bond developed between their similar glass-like structures and the lower friction stress in B1 with the presence of carbon. Whether, however, the carbon is formed by reaction between the silicon carbide of the fibre and oxygen from the glass to give a graphitic layer as reported by Cooper and Chyung [20], or whether it is a consequence of residues from the organic binder used in processing the composite cannot be ascertained. Clearly, more work is needed here.

4.4. The composite

The properties of the current series of Nicalon fibre reinforced Pyrex glass composites are controlled primarily by the cristobalite content, a high content causing premature brittle failure in composites with strong fibre–matrix bonds, and matrix disintegration in composites with weak fibre–matrix bonds. Hence, the first requirement which needs to be specified is that the cristobalite content should be kept to below 10 vol %. If this target can be achieved by control of the manufacturing process, then the composite properties will be governed essentially by the fibre–matrix interface. Here again the desired microstructure, as it is affected by composite processing, needs to be achieved and future work will focus upon ways of controlling interface characteristics, as they relate to the desired properties, by means of a better understanding of the relevant diffusion and reaction processes, particularly the role of carbon.

Acknowledgements

The authors would like to thank Rolls Royce plc and SERC for their support and the Rev. B. Chapman for assistance with the X-ray diffraction studies.

References

1. R. A. J. SAMBELL, D. H. BOWEN and D. C. PHILLIPS, *J. Mater. Sci.* 7 (1972) 663–675.
2. R. A. J. SAMBELL, A. BRIGGS, D. C. PHILLIPS and D. H. BOWEN, *ibid.* 7 (1972) 676–681.
3. D. C. PHILLIPS, R. A. J. SAMBELL and D. H. BOWEN, *ibid.* 7 (1972) 1454–1464.
4. S. YAJIMA, H. KAYANO, K. OKAMURA, M. OMORI, J. HAYASHI and K. AKUTSI, *Amer. Ceram. Soc. Bull.* **55** (1976) 1065.
5. S. YAJIMA, K. OKAMURA, J. HAYASHI and M. OMORI, *J. Amer. Ceram. Soc.* **59** (1976) 324–327.
6. K. M. PREWO and J. J. BRENNAN, *J. Mater. Sci.* **15** (1980) 463–468.
7. *Idem., ibid.* **17** (1982) 1201–1206.
8. D. M. DAWSON, R. F. PRESTON and A. PURSER, *Ceram. Engng Sci. Proc.* **8** (1987) 815–821.
9. B. A. FORD, R. G. COOKE and S. NEWSAM, *Brit. Ceram. Proc.* **39** (1987) 229–234.
10. A. BRIGGS and R. W. DAVIDGE, *Mater. Sci. Engng* **A109** (1989) 363–372.
11. D. B. MARSHALL and A. G. EVANS, *J. Amer. Ceram. Soc.* **68** (1985) 225–31.
12. H. P. KLUG and L. E. ALEXANDER "X-ray diffraction procedures for polycrystalline and amorphous materials" 2nd edn, (John Wiley, New York, 1974).
13. F. A. HABIB, R. G. COOKE and B. HARRIS, *Brit. Ceram. Trans. J.* **89** (1990) 115–124.
14. L. PORTE and A. SARTRE, *J. Mater. Sci.* **24** (1989) 271–275.
15. C. LAFFON, A. M. FLANK, P. LAGARDE, M. LARIDJANI, R. HAGEGE, P. OLRY , J. COTTERET, J. DIXMIER and J. L. MIQUEL, *ibid.* **24** (1989) 1503–1512.
16. V.S.R. MURTY and M. H. LEWIS, *J. Mater. Sci. Lett.* **8** (1989) 571–572.
17. M. B. VOLF "Technical Glasses", (Pitman, London, 1961).
18. W. K. TREDWAY, K. M. PREWO and C. G. PANTANO, *Carbon* **27** (1989) 717–727.
19. T. J. CLARK, E. R. PRACK, M. I. HAIDER and L. C. SAWYER, *Ceram. Engng Sci. Proc.* **8** (1987) 717–731.
20. R. F. COOPER and K. CHYUNG, *J. Mater. Sci.* **22** (1987) 3148–3160.

Received 19 March
and accepted 3 July 1990